Intraspecific variation in growth-related traits—from leaf to whole-tree—in three provenances of Cryptomeria japonica canopy trees grown in a common garden

Azuma, Wakana A.
Kawai, Kiyosada
Tanabe, Tomoko
Nakahata, Ryo
Hiura, Tsutom

(Citation)
Ecological Research,38(1):83-97

(Issue Date)
2023-01

(Resource Type)
journal article

(Version)
Accepted Manuscript

Special features “Functional biogeography: Lessons from the geographic variations in the most dominant tree species in Japan”

Intraspecific variation in growth-related traits—from leaf to whole-tree—in three provenances of *Cryptomeria japonica* canopy trees grown in a common garden

WAKANA A. AZUMA[1, 2, †, *]

KIYOSADA KAWAI[3, 4, †]

TOMOKO TANABE[5]

RYO NAKAHATA[2, 6]

TSUTOM HIURA[7]

[1] Graduate School of Agricultural Science, Kobe University, Kobe 657-8501, JAPAN

[2] Graduate School of Agriculture, Kyoto University, Kyoto 606-8502, JAPAN

[3] Center for Ecological Research, Kyoto University, Otsu 520-2113, JAPAN

[4] Forestry Division, Japan International Research Center for Agricultural Science (JIRCAS), Tsukuba 305-8686, JAPAN

[5] Graduate School of Global Environmental Studies, Kyoto University, Kyoto, 606-8501,

JAPAN

[6] Graduate School of Agricultural and Life Sciences, The University of Tokyo, 113-8657, JAPAN

[7] Department of Ecosystem Studies, The University of Tokyo, Tokyo, 113-8657, JAPAN

[†] WAA and KK should be considered joint first author.

*Corresponding author: Email: wakana@port.kobe-u.ac.jp, Phone: +81-78-803-5936

Abstract

To elucidate the physiological and morphological factors underlying intraspecific variation in growth rate, we examined the variation in leaf and whole-tree traits for three geographical variations of ca. 45-year-old Japanese cedar (*Cryptomeria japonica* D. Don) with contrasting heights and radial growth in a common garden. Traits that reflect leaf-level photosynthesis, water relations, and whole-tree level crown structure in relation to light use and hydraulic architecture were measured. Overall, intraspecific variation in growth characteristics in field-grown adult trees was regulated by whole-tree properties rather than leaf properties. Most leaf traits were similar among provenances. Nevertheless, the leaf traits exhibited highest maximum net photosynthetic rate, dark respiration rate, and light compensation point in provenances whose native habitats are most similar to the common garden in the present study. Together with previous reports that this provenance has higher root nutrient acquisition capacity than the other two provenances, it can be said that organ-level resource use strategies are coupled in a tandem manner. At the whole-tree level, hydraulic architecture—as explained by axial variation in the hydraulically-weighted tracheid diameter—can be linked to leaf distribution with respect to light use strategies as well as water transport capacity, leading to differences in growth characteristics among provenances. The study of intraspecific variation in growth

characteristics in trees with a wide range of native habitats is expected to be a useful indicator for predicting changes in growth potential and forest dynamics in response to climate change in each habitat.

Keywords: xylem anatomy, functional trait, photosynthesis, transpiration, hydraulic architecture

Introduction

The patterns and mechanisms of tree growth have long been the core research topics in tree physiology. The rate of tree growth is influenced by 1) the inherited characteristics of trees, such as size, phenology, and physiological properties (e.g., Kitajima 1994; Moreira et al. 2014; Obeso 2002; Poorter and Remkes 1990); 2) the surrounding abiotic and biotic factors, such as light availability, mycorrhizal symbiosis, and herbivore pressure (Coley and Barone 1996; Montgomery and Chazdon 2002; Wu and Xia 2006); and 3) their interactions (Nabeshima et al. 2010). To understand the mechanisms underlying the variation in the growth rate of trees, Hunt (1978) introduced the concept of growth analysis, where dry mass-based relative growth rate (RGR) is expressed as the net assimilation rate (NAR) multiplied by the leaf area ratio (LAR, total leaf area per unit whole-plant mass). This equation indicates that tree growth is governed by both leaf-level photosynthetic rate and whole-tree carbon allocation. Therefore, it is expected that any plant traits (physiological and morphological characteristics) influencing NAR and LAR could potentially cause variation in growth rate.

Water transport from the roots to leaves is a major determinant of photosynthetic capacity—and thus possibly NAR—because CO_2 absorption inevitably induces water loss due to transpiration (Brodribb 2009; Sperry 2003). Previous studies have

68 demonstrated that organ-level hydraulic conductivity strongly influences the maximum
69 photosynthetic rate (Brodribb and Feild 2000; Santiago et al. 2004) and growth rate (Fan
70 et al. 2012; Hietz et al. 2017; Poorter et al. 2010). Hydraulic conductivity is governed by
71 the morphology, dimensions (particularly the diameter), and spatial arrangements of the
72 conducting elements (vessels and tracheids) (Hacke et al. 2017; Tyree and Zimmermann
73 2002). The diameter of conducting elements varies according to tree size (Olson et al.
74 2014), environmental gradients (Arenas-Navarro et al. 2021, Zheng et al. 2022), and
75 position within trees (Petit et al. 2008; Spicer and Gartner 2001). The latter factor
76 determines the pattern of accumulation of hydraulic resistance along tree height, thus
77 influencing whole-tree hydraulic conductivity, especially in large trees (Liu et al. 2019).
78 Theoretical (Enquist 2003; West et al. 1999) and empirical (Anfodillo et al. 2006, 2013;
79 Olson et al. 2018; Williams et al. 2019) studies have shown that the diameter of
80 conducting elements increases from the stem tip to the base as $D = \alpha L^{\beta}$, where D is the
81 conduit diameter, L is the distance from the tree apex, and α and β are coefficients. This
82 increase in diameter possibly mitigates the negative effects of accumulating hydraulic
83 resistance on tree growth and photosynthesis (Ryan and Yoder 1997). Here, if $\beta \geq 0.20$,
84 metabolic theory predicts that accumulated hydraulic resistance would be nearly
85 independent of L; in such cases, trees can maintain their metabolism with an increase in

86 height (Enquist 2003; West et al. 1999). Accordingly, the variations in α and β should
87 reflect the differences in whole-tree hydraulic architecture, and thus the growth rate
88 (Rosell et al. 2017).

89 In addition to leaf-level photosynthetic capacity, the LAR also affects the RGR
90 of trees (Givnish 1988; Kitajima 1994; Poorter and Remkes 1990). The LAR can be
91 further decomposed into specific leaf area (SLA) multiplied by the leaf mass fraction
92 (LMF, leaf mass per unit whole-tree mass). Therefore, both leaf morphology and carbon
93 allocation to leaves influence the LAR. Leaf dry mass per area (LMA, the inverse of SLA)
94 is often negatively correlated with RGR across species (e.g., Gibert et al. 2016; Iida et al.
95 2014; Poorter et al. 2006). With regard to LMF, biomass distribution among organs
96 reflects the volume and density of each organ (leaves, stems, branches, and roots). Large
97 trees (> 1,000 kg) generally allocate most of the biomass (> 70%) to stem wood (Poorter
98 et al. 2015). Therefore, for a given amount of photosynthate and SLA, an increase in wood
99 density at the stem increases biomass allocation to the stem (King et al. 2006), thus
100 reducing LMF and RGR. At the whole-tree level, high allocation of biomass to stems
101 reduces LAR, and thus constrains RGR (Onoda et al. 2014).

102 To date, attempts to identify the traits underlying the RGR of trees in relation to
103 NAR and LAR have focused on interspecific variation, mostly using different

104 phylogenies (e.g., King et al. 2006; Martínez-Vilalta et al. 2010; Poorter and Remkes
105 1990; Wright et al. 2010). However, few studies have dealt with intraspecific variations.
106 Because evolutionary processes do not produce extreme phenotypes at smaller temporal
107 scales, intraspecific trait variation is often similar to or lower than interspecific variations
108 (e.g., Asner et al. 2014; Messier et al. 2010). Investigating such within-species variations
109 requires the following: 1) establishing the evolutionary robustness of trait–growth
110 relationships, and 2) investigating an extensive suite of traits that may contribute to a
111 mechanistic and comprehensive understanding of tree growth (Medeiros et al. 2019).
112 Although the importance of LAR-associated traits (e.g., LMA and wood density) on
113 growth is well appreciated, few studies have examined them together with leaf-level
114 physiological traits, particularly for field-grown large trees. In practical terms, this type
115 of within-species approach is ideal for species that show wide distribution ranges—
116 including heterogeneous resource availabilities—because variation in local environments
117 would cause divergent selections in traits and associated growth rates, providing
118 opportunities to test their evolutionary correlations (Cavender-Bares 2019). The Japanese
119 archipelago is a suitable area for this type of study, as it encompasses a wide
120 environmental gradient that causes high intraspecific variation in phenotypic traits (e.g.,
121 Ishii et al. 2018; Osada et al. 2015; Tateishi et al. 2010).

Here, we chose the natural geographical variations of the Japanese cedar (*Cryptomeria japonica* D. Don), which dominates about 20% (including plantation forests) of Japan's forest area (Forestry Agency of Japan 2011) as a study clade. We examined the intraspecific variations in leaf and whole-tree traits associated with NAR and LAR in relation to their growth rate in a common garden. *C. japonica* is widely distributed in the Japanese archipelago (from 30°15′ N to 40°42′ N) and comprises genetically differentiated provenances (Tsumura et al. 2012, 2014) that differ in morphology, growth rate, allometries, and other functional traits (Hiura et al. 2021; Nishizono et al. 2014; Osone et al. 2021). Thus, this species is ideal for testing trait–growth relationships at the intraspecific level. A previous study conducted in the same common garden had shown that the root exudation rate and nutrient status of leaves and roots were higher in provenances with a high growth rate, indicating that adaptive divergence in nutrient-uptake strategies among provenances causes a difference in growth rates (Ohta et al. 2019). Based on this, we tested the prediction that provenances in which leaf and whole-tree traits are associated with high NAR (e.g., high photosynthetic rate, conductive tracheid, and high nitrogen content) and high LAR (e.g., low LMA, low wood density, and high fraction of leaf mass) show high RGR in terms of height and diameter. We measured 25 leaf and whole-tree traits that are associated with NAR and LAR through

140 their influence on the resource use strategies of light, water, and nutrients (e.g., leaf
141 photosynthetic rate, crown structure, and tree hydraulic architecture). Using these data,
142 we compared the traits among three provenances of ca. 45-year-old *C. japonica* with
143 different genotypes and contrasting RGR grown under the same environment.
144
145 **Methods**
146 *Study site and plant materials*
147 The study was conducted in a common garden of *C. japonica* established at the
148 Wakayama Experimental Forest of Hokkaido University in Wakayama Prefecture, Japan
149 (33°40′ N, 135°40′ E, and 240 m above sea level). This forest is covered by a very thin
150 and weakly developed mineral soil without horizon differentiation (Regosol, based on the
151 World Reference Base for Soil Resources) (Kanda et al. 2018). The mean annual
152 precipitation and temperature from 1985 to 2019 were 3,564 mm and 14.7°C, respectively
153 (Japan Meteorological Agency).
154 The common garden was located on a south-facing slope, and the soil color
155 (gray), texture (silt and gravel), and depth (< 10 cm) were uniform across the slope. In
156 the common garden, *C. japonica* grown in various regions of Japan were planted with
157 similar densities (ca. 2,000 individuals per hectare) between 1967 and 1973. The stand

158 had not been managed after planting until our field survey, and the canopy was closed
159 without any gaps. Here, we used clonal stands of the three provenances that had also been
160 used in Ohta et al. (2019): Yoshino, Yanase, and Yaku. These provenances were planted
161 within 50 m of each other at the upper, middle, and lower parts of the slope, respectively.
162 The native habitats of all three provenances are located in the southwestern part of Japan
163 (Figure 1). As in the common garden, all native habitats are covered with very thin soils
164 due to high precipitation and steep slopes, but the basement rock of each native habitat is
165 different (sedimentary rock in Yoshino, sandstone and shale in Yanase, and granite in
166 Yaku) (Geological Survey of Japan 2015). Yoshino and Yanase are known to have
167 relatively high growth rates in the early stage of growth (< ca. 50 years old), whereas
168 Yaku has low growth rates (Itaka et al. 2013; Nishizono et al. 2014). These growth
169 patterns were also observed in the mean tree height and diameter at breast height (DBH)
170 of each provenance measured across the common garden of the present study in 2015:
171 18.3 m and 23.1 cm in Yoshino (n = 100), 15.4 m and 19.2 cm in Yanase (n = 193), and
172 10.9 m and 18.6 cm in Yaku (n = 119), respectively. The age of stands from each
173 provenance in 2015 was 49 years in Yaku, 46 years in Yanase, and 43 years in Yoshino.
174 In this study, three individuals of each provenance were cut down from their
175 stem base at noon on a sunny day in August 2018 and used for the measurements

176 described below. The canopy tops of each sample tree were exposed to direct sunlight.
177 We stretched a tape measure along the stem to measure the tree height, crown depth, and
178 height and diameter of the primary branches attached to the stem of each individual,
179 except for one Yaku tree. The mean height and DBH of the sample trees for each
180 provenance were 21.1 m and 22.7 cm in Yoshino, 20.9 m and 25.6 cm in Yanase, and 11.8
181 m and 15.7 cm in Yaku, respectively. To calculate the stem volume of each individual,
182 stem disks (approximately 1 cm in thickness) were collected at 5 m intervals starting from
183 a height of 1.3 m along the stem. The diameters were recorded, and the stem volume was
184 calculated as the sum of the truncated cones.
185
186 *Growth characteristics and tree structures*
187 To estimate the recent growth characteristics of each provenance, the annual
188 stem height and radial growth rates (G_h and G_r, cm yr^{-1} and mm yr^{-1}) from 2013 to 2016
189 were measured from the annual shoot length at the top of each tree crown (except for one
190 individual from Yoshino, which could not be measured because the tip of the trunk was
191 unclear). These measurements were recorded with an accuracy of 1 mm. The annual ring
192 width was measured from one direction of the stem disk at a height of 1.3 m with an
193 accuracy of 0.001 mm. Based on the above data, we calculated the relative growth rate

for height (RGR_h, yr^{-1}) and DBH (RGR_r, yr^{-1}) from 2013 to 2016 using the following equation (Hunt 1982), assuming that both show exponential growth:

$$\frac{\ln(X_j)-\ln(X_i)}{t_j-t_i} \quad \text{Eqn. 1}$$

where X_j and X_i are the height or DBH at times j and i, respectively (when annual growth ceases), and t_j and t_i are the years. G_h, G_r, RGR_h, and RGR_r were calculated for each year-interval (2013–2014, 2014–2015, 2015–2016) for individual trees.

One woody core (ca. 3 cm in length from the cambium) was collected from the main stem at DBH using an incremental borer (5.15 mm in diameter; Haglöf, Langsele, Sweden) from 10–12 individuals per provenance in August 2019. This woody core was used to calculate the sapwood density (WD, g cm^{-3}). The sapwood volume was measured from the diameter and length of a core (assuming a cylindrical shape), and the bark and heartwood portions (based on the visual check) were removed with a razor blade before measurement. All samples were oven-dried (65°C, > 72 h), and their dry masses were recorded. The volumetric density of the sapwood was then calculated as the dry mass divided by its fresh volume.

The crown architecture was evaluated by the absolute crown depth (CD, m), and the ratio of CD to tree height (RCD, m m^{-1}) was calculated for each individual. In addition, we assumed a pipe model, in which the ratio of leaf area to the cross-sectional

212 area of the branch base is constant (Shinozaki et al. 1964). Based on this, we calculated
213 the total cross-sectional area per stem volume (TBA, $cm^2\ m^{-3}$) of primary branch bases
214 for each individual as an alternative index of LAR.
215
216 *Tree hydraulic architecture*
217 To analyze the stem anatomy, we excised one sample from the cambium (approximate
218 length, 2 cm; width, 1 cm; depth, 1–2 cm) from all the stem disks we collected, avoiding
219 the reaction wood part. Subsequently, transverse sections (approximate thickness, 30–40
220 μm) were prepared using a sliding microtome (Figure 2). The samples were stained with
221 0.5% (w/v) safranin in 50% ethanol and dehydrated using an ethanol series (50%, 99.5%,
222 and 100%). Finally, the samples were dehydrated in xylene and mounted on glass slides
223 with Canada balsam. Images were captured using a digital camera (EOS kiss X3, Canon,
224 Tokyo, Japan) coupled to a light microscope (BX50, Olympus, Tokyo, Japan). The
225 resolution of the images was 1919 pixels mm^{-1} with a full size of approximately 1.2 mm
226 × 0.8 mm. Using these images, we measured the tracheid density (TD, mm^{-2}) of
227 earlywood and the mean tracheid lumen area (TLA, μm^2) for > 650 tracheids per image
228 using the Fiji image processing software (Schindelin et al. 2012). The disjunction between
229 earlywood and latewood followed Mork's definition (Denne 1988): latewood was defined

as the wood with the ratio of lumen diameter and double wall thickness < 2. The TLA was convened to the tracheid diameter (D, μm) by assuming circular cross-sections, and the mean hydraulically-weighted tracheid diameter (D_h, μm) of every stem disk was calculated as follows (Tyree and Zimmermann 2002):

$$D_{\mathrm{h}} = \left(\frac{1}{n}\sum_{i=1}^{n} D^4\right)^{\frac{1}{4}} \quad \text{Eqn. 2}$$

where n is the number of tracheids.

In a soil–plant hydraulic continuum, water flow occurs in proportion to the water potential gradient and is inversely proportional to the hydraulic conductivity according to Darcy's law (Sperry et al. 1998). To estimate the potential water flow in the whole tree, we calculated the water potential gradient from the difference between Ψ_{TL} and Ψ_R, as described below. The potential specific xylem conductivity at a certain height (K_p, kg m^{-1} s^{-1} MPa^{-1}) was calculated according to (Poorter et al. 2010):

$$K_{\mathrm{p}} = \left(\frac{\pi\rho_W}{128\eta}\right) TD * D_h^4 \quad \text{Eqn. 3}$$

where ρ_w is the density of water at 20°C (998.2 kg m^{-3} at 20°C), η is the viscosity of water at 20°C (1.002 × 10^{-3} Pa s at 20°C), and TD and D_h are as described above.

We calculated K_p at different heights from every stem disk, and then the axial variation-weighted potential specific xylem conductance (K_{ap}, kg m^{-2} s^{-1} MPa^{-1}) and potential transpiration rate per unit sapwood area (E_p, kg m^{-2} s^{-1}) were estimated. Because

of the decrease in D_h from the stem base to the treetop (Figure S1a), K_p decreased as sampling height increased in each tree, and its variation was relatively well explained by linear regressions (R^2 = 0.53–1.00, Figure S1b). These patterns allow us to express the minimum specific resistivity (R_{min}, an inverse of K_p) as a function of height as follows:

$$R_{\mathrm{min,i}} = \frac{1}{a_i H + b_i} \quad \text{Eqn. 4}$$

where $R_{min,i}$ H, a_i, and b_i are the R_{min}, height, and coefficients of tree i, respectively. Integrating R_{min} from the ground to the individual tree height yielded the minimum cumulative specific resistivity of the stem (R_{cum_min}, m^2 s MPa kg^{-1}), and potential specific xylem conductance (K_{ap}) was calculated as the inverse of R_{cum_min}. The E_p was calculated as K_{ap} multiplied by the water potential gradient from the roots to the treetop ($\Psi_R - \Psi_{TT}$, MPa). The above calculations assumed that most water movements occur in the earlywood at the outermost sapwood where large tracheids are observed; thus, we considered our results to be robust to the radial variation of tracheid anatomy.

Leaf water relations

After cutting down the trees in the common garden as described above, the daytime water potential of treetop leaves (Ψ_{TL}, MPa), lowest-crown leaves (Ψ_{LL}, MPa), and fine roots (Ψ_R, MPa) were immediately measured for three replicates per individual using a pressure

266 chamber (Model 1000, PMS Instruments, Corvallis, USA). Branches (ca. 30 cm in length)
267 were sampled from the treetop of each individual, immediately recut in bucketed water,
268 and covered with a black plastic bag overnight in the laboratory for the pressure–volume
269 measurement.

270 The pressure–volume curve of the leaves (second- and current-year internodes;
271 three shoots per provenance) was obtained using the bench-drying approach for the
272 pressure–volume technique (Tyree and Hammel 1972). Using a pressure chamber (Model
273 1000, PMS Instruments, Corvallis, USA), we repeatedly measured the leaf water potential
274 (Ψ_L, MPa) and fresh mass (M_F, g) of the sampled leaves (repeat pressurization method,
275 Hinckley et al. 1980, Parker and Colombo 1995). After the pressure–volume
276 measurement, all the sample shoots were photographed to measure the total leaf surface
277 area (A_L, m^2), as described below. Next, the leaves were oven-dried to constant weight at
278 65°C for 48 h to obtain the leaf dry mass (M_D, g). To estimate the drought tolerance of
279 shoots, we calculated the osmotic potential at saturation (Ψ_{sat}, MPa), osmotic potential at
280 turgor loss (Ψ_{tlp}, MPa), and relative water content at turgor loss (RWC_{tlp}) at the bulk shoot
281 level using the pressure–volume curve. The saturated leaf water content (M_W = MF –
282 MD) was used to calculate leaf hydraulic capacitance (C_L, mol m^{-2} MPa^{-1}) and succulence
283 (S_L, g H_2O m^{-2}).

$$C_L = (\delta RWC/\delta \Psi_L)\ (M_D/A_L)\ (M_W/M_D) / MW \quad \text{Eqn. 5}$$

$$S_L = M_W/A_L \quad \text{Eqn. 6}$$

where $\delta RWC/\delta \Psi_L$ is the slope of the Ψ_L–RWC relationship calculated from the pressure–volume curve before the turgor loss point, and MW is the molecular weight of water.

Leaf morphology

After the pressure–volume measurement, each sample shoot (three shoots per provenance) was placed on a slide viewer, illuminated from below, and photographed to obtain the shoot silhouette images. All leaves were detached from the shoot axis, laid on the slide viewer without overlap, and photographed. The photographs of the shoots and leaves were analyzed using the ImageJ image analysis software (Schneider et al. 2012) to quantify the shoot silhouette area (A_S, m^2) and projected leaf area (A_P, m^2). To obtain A_L, the perimeter-to-width ratios obtained from the transverse sections of leaves were multiplied by A_P (Azuma et al. 2016). We calculated the leaf mass per area (LMA = M_D/A_P, g m^{-2}) and shoot silhouette area to projected leaf area ratio (SPAR = A_S/A_P, a measure of leaf overlap within the shoot).

Leaf photosynthetic traits

In August 2019, we sampled a branch (approximate length, 30 cm) from the treetop of each individual tree using a long sickle. The branch was immediately recut under water and fully rehydrated in the laboratory for photosynthetic measurement. The gas exchange of second-year shoots was measured in all sampled branches (three branches per provenance) using the LI-6400 portable gas exchange system fitted with an LI-6400-05 conifer chamber (Li-Cor Inc., Lincoln, NE, USA). The air temperature and CO_2 concentration in the cuvette were maintained at 25°C and 380 ppm, respectively. We used an external halogen-type light source fitted with a profile spot projection lens (MHAB-150W and ML-50, Moritex Corp., Tokyo, Japan) to provide parallel beam radiation with a maximum photosynthetic photon flux density (PPFD) of 1600 μmol m^{-2} s^{-1}. We varied the light intensity to obtain the photosynthetic light response curve for each shoot.

Following these measurements, the leaves inside the conifer chamber (10 cm^2) were carefully cut out and photographed to measure the projected leaf area using Image J (Schneider et al. 2012). The leaves were then oven-dried to a constant mass to determine the leaf dry mass. We estimated maximum net photosynthetic rate (P_{max}, μmol CO_2 m^{-2} s^{-1}), dark respiration rate (R, μmol CO_2 m^{-2} s^{-1}), and light compensation point (L_C, μmol m^{-2} s^{-1} PPFD) from the relationship between light intensity and net photosynthetic rate.

These measurements were conducted using the Light Response Curve software developed by Li-Cor Inc. (Norman et al. 1992). We also calculated maximum photosynthetic rate per leaf dry mass ($P_{max\_mass,}$ nmol CO_2 g^{-1} s^{-1}) by dividing P_{max} by LMA.

To evaluate the long-term photosynthetic water-use efficiency, we measured the leaf carbon isotope ratio ($\delta^{13}C$, ‰) in 9–10 individuals of each provenance from which we had collected stem cores (Farquhar et al. 1989). The leaves were oven-dried (65°C, > 72 h) and then ground using a mill. Then, $\delta^{13}C$ was measured using an isotope ratio mass spectrometer (DELTA V Plus and DELTA V Advantage, Thermo Fisher Scientific, Massachusetts, USA) at the Center for Ecological Research (CER), Kyoto University. Simultaneously, the dry mass-based leaf nitrogen and carbon concentrations (N_{mass} and C_{mass}, %) were measured using an elemental analyzer (Flash 2000, Thermo Fisher Scientific) coupled to an isotope ratio mass spectrometer.

Statistical analysis

All analyses were performed using R (R Core Team 2019, R version 3.6.1). To calculate K_{ap} and E_p, we first estimated coefficients *a* and *b* in Eqn. 4 for each tree with nonlinear least square regression analyses using the R function 'nls'. Using these values, we integrated Eqn. 4 from 0 (ground) to tree height for each tree to yield R_{cum_min} using the

337 'integrate' function in the R package 'stats' (version 4.1.2).

338 To examine the differences in the leaf, stem, and whole-tree traits among
339 provenances, we used one-way ANOVA followed by Tukey's HSD post hoc tests. We also
340 examined the residual plots of linear regressions for each trait. When the data did not meet
341 the assumptions of ANOVA (normality and homogeneity of variances), we instead
342 conducted the Kruskal–Wallis test followed by the Steel–Dwass test. To compare G_h, Gr,
343 RGR_h, and RGR_r, we first calculated the average provenance-by-year values to consider
344 the variation in growth among years, and then examined the differences among
345 provenances based on the linear mixed model analyses with a restricted maximum
346 likelihood (REML) estimation, where provenance was fixed effect and year was a random
347 intercept, using the R package 'lme4' (Bates et al. 2015). Following this, we examined
348 the differences among provenances using linear mixed model analyses (with provenance
349 as a fixed effect and year being a random intercept) using the R package 'lme4' (Bates et
350 al. 2015). The model parameters were calculated by REML estimation.

351 To examine the axial variation of D_h, we converted the sampling height to the
352 distance from the tree apex (L), thus enabling comparisons among trees of different
353 heights. We estimated the slope (basipetal conduit widening rate, β) and intercept (log D_h
354 at 1 m below the treetop, α) of L–D_h relationships among provenances based on linear

mixed model analyses, where L, provenance, and their interaction were fixed effects and individual trees had a random intercept. The model parameters were calculated using REML estimation. Here, we $\log_{10}$-transformed D_h and L prior to analyses to reflect the scaling relationship of D_h with L (see Introduction). The same analysis was performed by substituting L with the relative distance from the treetop or stem diameter at sampling height to estimate the effect of size differences among provenances on tracheid tapering. We also calculated marginal and conditional R^2 (R_m^2 and R_c^2, respectively, Nakagawa and Schielzeth 2013) to evaluate the model fit using the R package 'MuMIN' (Barton 2016). We set a significance level of 0.05.

Results

Growth characteristics and tree structures

G_h, G_r, RGR_h, and RGR_r were the lowest in the Yaku provenance, followed by Yoshino and Yanase (Table 1). Correspondingly, WD was highest in Yaku, followed by Yoshino, and then Yanase (Table 2). CD was larger in Yanase than in Yaku. RCD was not significantly different among the provinces; however, there was a trend of Yanase having a higher RCD compared to the other two provenances (Table 2). TBA was significantly higher in Yaku than in Yanase and Yoshino.

373

374 *Axial variation of tracheid diameter and whole-tree hydraulics*

375 For all provenances, the D_h was generally smallest near the top of the tree, and the largest
376 D_h was found near the stem base (Figure 3, Table 3). The slope (basipetal conduit
377 widening rate, β) and intercept (log D_h at 1 m below the treetop, α) in the L–D_h
378 relationship were significantly different between provenances (Table 3): β was higher in
379 Yanase and Yoshino than in Yaku, whereas α was higher in Yaku than in the other two.
380 Yanase had a marginally higher β than Yoshino ($p = 0.076$). In addition, provenances with
381 high β tended to exhibit low α. The overall model fit was relatively good (both R_m^2 and
382 $R_c^2 = 0.85$). We also found that on average, provenances with higher β had longer CD (R^2
383 $= 0.999$, $p = 0.021$, $n = 3$), indicating a link between hydraulics and crown architectures
384 at the whole-tree level (Figure 3). However, when we substituted L with the relative
385 distance from the tree top or stem diameter at the sampling height, the slope was not
386 significantly different among provenances in either case (R_m^2 and $R_c^2 = 0.73$, Table S1,
387 for relative distance; $R_m^2 = 0.72$, $R_c^2 = 0.76$, Table S2 for diameter). This suggested that
388 the results in the L–D_h relationship may reflect different sizes among provenances.

389 A decline in D_h caused a decline in K_p along tree height with indistinguishable
390 slopes among provenances ($p = 0.77$, Figure S1). These patterns led to significant positive

391 correlations between total tree height and R_{cum_min} across trees (p = 0.003, Figure S2).
392 Consequently, despite having the lowest β, Yaku had the highest K_{ap} because it also had
393 the lowest tree height. Despite the high K_{ap} in Yaku, E_p was not significantly different
394 among provenances (p = 0.28), as it was offset by the relatively small $\Psi_{TL} - \Psi_R$ in Yaku
395 (Table 2).
396
397 *Leaf water relations, morphology, and photosynthetic traits*
398 Leaf water relations and leaf morphology were similar, with no significant differences
399 among provenances (Table 2). Although most leaf photosynthetic traits were not
400 significantly different between provenances, there were significant or marginally
401 significant differences in R (p = 0.042), Lc (p = 0.053), and $\delta^{13}C$ (p = 0.054) among
402 provenances. R and Lc were highest in Yoshino and lowest in Yanase, whereas $\delta^{13}C$ was
403 highest in Yaku and lowest in Yanase (Table 2).
404
405 **Discussion**
406 Here, we compared the traits of three provenances of ca. 45-year-old *C. japonica* with
407 different genotypes and contrasting RGR (Yaku, Yanase, and Yoshino) grown under the
408 same environment. Our results partially supported our prediction that the trees in the

409 resource-acquisitive provenance achieved higher growth rates. Among the traits affecting
410 NAR and LAR that lead to differences in RGR, leaf traits had similar values among
411 provenances, whereas canopy structure and hydraulic architecture at the whole-tree level
412 were different between provenances.

413 The life-history theory suggests that organ-level resource use strategies are
414 coupled in a tandem manner (Grime et al. 1997; Reich 2014). The previous studies
415 conducted in the same common garden showed the highest rate of root exudation in
416 Yoshino whose native habitat was most similar to the common garden (Ohta et al. 2019).
417 It has been speculated that this is a result of adaptation to the basement rock in its native
418 habitat. In support of the life-history theory, Yoshino showed resource-acquisitive leaf
419 traits, such as the highest P_{max}, R, and L_c among the three provenances in the present study
420 (Table 2). In turn, the lowest Lc in Yanase may allow Yanase to distribute their leaves in
421 the lowest position relative to tree height. In *C. japonica*, photosynthetic parameters such
422 as P_{max}, V_{cmax}, and nitrogen content in the second-year (former current year) shoots
423 decrease after summer and primary photosynthetic sites shift to current-year shoots as the
424 seasons changed (Inoue et al. 2018, Kobayashi et al. 2010, Tobita et al. 2014).
425 Considering that the P_{max} in the present study was measured on the second-year shoots, it
426 would be reasonable that P_{max} was lower than that measured on the current year shoots of

427 *C. japonica* in general (Osone et al. 2021). P_{max} was similar among provenances, but the
428 leaf water-use efficiency (estimated by $\delta^{13}C$) tended to be higher in Yaku with lower
429 growth rate (Tables 1 and 2). Leaf water-use efficiency estimated by $\delta^{13}C$ represents long-
430 term accumulation of the photosynthesis per unit stomatal conductance (Farquhar et al.
431 1989). The high leaf water-use efficiency in Yaku may be partially due to low basipetal
432 conduit widening rate (β), which negatively affects photosynthesis and growth at the
433 whole-tree level through the accumulation of hydraulic resistance from stem anatomical
434 traits as discussed below. However, most leaf water relations, morphology, and
435 photosynthetic traits were similar among provenances (Table 2), indicating that growth-
436 related traits at the leaf level alone did not describe differences in RGR among
437 provenances.

438 In terms of growth characteristics, Yaku trees showed the lowest stem height,
439 radial growth rate, and RGR, corresponding to the highest sapwood density (Tables 1 and
440 2). The high WD in Yaku was also associated with a small tracheid diameter at the same
441 height compared to the two other provenances (Figure S1a). WD is negatively related to
442 volumetric growth and positively related to strength (e.g., van Gelder et al. 2006; Poorter
443 et al. 2003); therefore, the high WD in Yaku may represent a genetically differentiated
444 trait in response to the limited tree size due to typhoon-induced canopy disturbance in its

native habitat (Ishii et al. 2010; Takashima et al. 2009). In addition, WD can influence LAR, which is related to tree growth rate (Givnish 1988; Kitajima 1994; Poorter and Remkes 1990). High biomass allocation to the stem affected the variation in WD and could be predicted to reduce LAR, leading to constrained RGR (Poorter et al. 2010; Wright et al. 2010). However, the large TBA in Yaku (Table 2) indicated that assuming a pipe model, the biomass allocation to leaves was higher (Shinozaki et al. 1964) when assuming no difference in leaf area relative to the cross-sectional area of the branch base among provenances. However, the foliage was concentrated at a relatively higher position on the stem. Coniferous trees generally allow light to penetrate deeper into the canopy compared to broadleaf trees because of the arrangement of shoots and branches (Ishii and Asano 2010). Multi-layered trees with branches distributed throughout the crown typically show lower efficiency of light interception compared to that in single-layered trees with branches distributed in the upper canopy. However, the productive leaf area is theoretically maximized by maintaining a deep canopy in conifer trees (Onoda et al. 2014; Niinemets 2010; Stenberg 1996). In turn, the crown structure with low light-use efficiency may be related to the low RGR in Yaku trees.

At the whole-tree level, the tree hydraulic architecture affecting photosynthetic capacity also differed between Yaku and the other two provenances. The rate of basipetal

463 conduit widening (β) describes how conduits widen from the treetop per unit stem length.
464 The value of β converges to 0.2 as the predicted exponent in the WBE (West, Brown and
465 Enquis) model in a very broad-leaved plant species. In contrast, $\beta < 0.2$ results in a
466 decreased conduit widening rate and increased resistance to sap flow within the whole
467 tree (Rosell et al. 2017). In the present study, β was 0.17 in Yanase, 0.13 in Yoshino, and
468 0.07 in Yaku (Figure 3, Table 3). These values were lower than the optimal value for water
469 transport (0.2), which may be partly due to the need for coniferous tracheids to perform
470 water transport and achieve mechanical stability. However, the β converges to 0.2 in the
471 world's tallest tree species—*Sequoia sempervirens* and *Sequoiadendron giganteum*
472 (height, 86–105 m)—suggesting the significant contribution of basipetal conduit
473 widening as a hydraulic compensation mechanism with increasing tree height. In other
474 words, trees that can achieve the optimal β show a higher maximum height (Williams et
475 al. 2019). Because the size-dependence of cumulative water resistance decreases as β
476 approaches 0.2, Yanase trees can maintain a high potential for tree growth, resulting in a
477 high maximum height. In Yaku, β was significantly smaller than in the other two
478 provenances, and thus tree height could be constrained as the tree size increased. In
479 addition, there was a negative correlation between β and α (log D_h at 1 m below the
480 treetop) in the L–D_h relationship among the three provinces (Figure 3, Table 3),

481 suggesting that the possible hydraulic architecture of the whole tree is intraspecific
482 constrained. If the water requirement is high (for example, if the leaf area is large), the
483 tracheid diameter at the treetop (α) is predicted to be large even at the same stem length
484 (Olson et al. 2021). The advantage of a high α would be that a large tracheid diameter can
485 be maintained, such that the crown can have high water demand even in the upper part of
486 the stem. Indeed, foliar branches were concentrated at relatively high positions in Yaku,
487 whereas Yanase and Yoshino had a wide and sparse distribution deep into the stem (Table
488 2). We found that the higher β in Yanase was related to the long vertical distribution of
489 foliar branches along the stem (Figure 3). Thus, whole-tree hydraulic architecture—as
490 explained by axial variation in the hydraulically-weighted tracheid diameter—can be
491 linked to leaf distribution with respect to light use strategies as well as water transport
492 capacity, leading to differences in growth characteristics among provenances. In the
493 present study, only trees originating from Pacific regions with high precipitation were
494 used. However, comparisons with provenances with low precipitation may also be helpful
495 in understanding the wider patterns of variation in the functional traits of a tree species.
496 Interestingly, although there were evident differences in the tree hydraulic
497 structure, the potential transpiration rate per unit sapwood area (E_p) did not differ
498 significantly among the provenances (Table 2). Despite having the lowest β value, Yaku

had the lowest tree height, that is, a shorter L and less cumulative resistance of the whole tree. As a result, the potential specific xylem conductance (K_{ap}) was higher in Yaku trees than in Yanase and Yoshino; however, this was offset by a smaller water potential gradient from the roots to the treetop ($\Psi_R - \Psi_{TT}$). It remains to be seen whether E_p is constant in response to the growth environment, or whether it just happens to be constant as a result of the integration of genetic trait differences in each provenance. Future comparative studies on growth-related traits are required at the leaf and whole-tree levels in native habitats.

Conclusion

C. japonica is geographically widespread in Japan. In this species, intraspecific variation in growth characteristics in field-grown adult trees is regulated by whole-tree properties. Leaf traits were similar among the provenances in the same environments; nevertheless, in provenances whose native habitats were most similar to the common garden used in the present study, resource-acquisitive leaf traits were achieved through a combination of the high nutrient acquisition capacity of roots. Furthermore, the high rate of basipetal conduit widening was correlated with the long crown depth, suggesting that the light capture strategies at the whole-tree level are coordinated with hydraulic architectures,

possibly to achieve the optimal growth rate for each provenance. Based on our findings, we suggest that of the mechanisms underlying intraspecific variation in the growth characteristics of trees with a wide range of native habitats can be a useful indicator for predicting changes in growth potential and forest dynamics in response to climate change in each habitat.

Acknowledgements

We thank Dr. T. Ohta, and staff members of Wakayama Experimental forest, Hokkaido University, for help of field measurement on this study. The present study was conducted using Cooperative Research Facilities (Isotope Ratio Mass Spectrometer) of Center for Ecological Research, Kyoto University. This research was funded by JSPS KAKENHI Grant Number to TH (21H02227 and 21H05316) and JSPS Research Fellowships for Young Scientists to WAA (17J05154) and KK (20J01359).

Conflict of interest

None declared.

References

535 Anfodillo T, Carraro V, Carrer M, et al (2006) Convergent tapering of xylem conduits in
536 different woody species. New Phytologist 169:279–290. doi: 10.1111/j.1469-
537 8137.2005.01587.x
538 Anfodillo T, Petit G, Crivellaro A (2013) Axial conduit widening in woody species: A
539 still neglected anatomical pattern. IAWA Joural 34:352–364. doi:
540 10.1163/22941932-00000030
541 Arenas-Navarro, M., Oyama, K., García-Oliva, F., Torres-Miranda, A., De La Riva, E.
542 G. & Terrazas, T. (2021) The role of wood anatomical traits in the coexistence of
543 oak species along an environmental gradient. AoB PLANTS, 13, 6, 1–14. doi:
544 10.1093/aobpla/plab066
545 Asner GP, Martin RE, Tupayachi R, et al (2014) Amazonian functional diversity from
546 forest canopy chemical assembly. Proceedings of the National Academy of
547 Sciences of the United States of America 111:5604–5609. doi:
548 10.1073/pnas.1401181111
549 Azuma W, Ishii HRR, Kuroda K, Kuroda K (2016) Function and structure of leaves
550 contributing to increasing water storage with height in the tallest *Cryptomeria*
551 *japonica* trees of Japan. Trees—Structure and Function 30:141–152. doi:
552 10.1007/s00468-015-1283-3

553 Bartoń K (2016) MuMIn: Multi-Model Inference. R package version 1.43.17.
554 Bates D, Mächler M, Bolker BM, Walker SC (2015) Fitting linear mixed-effects models
555 using lme4. Journal of Statistical Software 67:1–48. doi: 10.18637/jss.v067.i01
556 Brodribb TJ (2009) Xylem hydraulic physiology: The functional backbone of terrestrial
557 plant productivity. Plant Science 177:245–251. doi: 10.1016/j.plantsci.2009.06.001
558 Brodribb TJ, Feild TS (2000) Stem hydraulic supply is linked to leaf photosynthetic
559 capacity: evidence from New Caledonian and Tasmanian rainforests. Plant, Cell &
560 Environment 23:1381–1388. doi: 10.1046/j.1365-3040.2000.00647.x
561 Cavender-Bares J (2019) Diversification, adaptation, and community assembly of the
562 American oaks (Quercus), a model clade for integrating ecology and evolution.
563 New Phytologist 221:669–692. doi: 10.1111/nph.15450
564 Coley P, Barone J (1996) Herbivory and plant defenses. The Annual Review of Ecology,
565 Evolution, and Systematics 27:305–335. doi: 10.1146/annurev.ecolsys.27.1.305
566 Denne MP (1988) Definition of latewood according to Mork (1928). IAWA J 10:59–62.
567 Enquist BJ (2003) Cope's rule and the evolution of long-distance transport in vascular
568 plants: Allometric scaling, biomass partitioning and optimization. Plant, Cell &
569 Environment 26:151–161. doi: 10.1046/j.1365-3040.2003.00987.x
570 Fan ZX, Zhang SB, Hao GY, et al (2012) Hydraulic conductivity traits predict growth

571 rates and adult stature of 40 Asian tropical tree species better than wood density. J
572 Ecol 100:732–741. doi: 10.1111/j.1365-2745.2011.01939.x
573 Farquhar GD, Ehleringer JR, Hubick KT (1989) Carbon isotope discrimination and
574 photosynthesis. Annu Rev Plant Physiol Plant Mol Biol 40:503–537. doi:
575 10.1146/annurev.pp.40.060189.002443
576 Forestry Agency of Japan. 2011. 2011 Forestry census. Tokyo: Forestry Agency.
577 Geological Survey of Japan. AIST (ed.) (2015) Seamless digital geological map of
578 Japan 1: 200,000. May 29, 2015 version. Geological survey of Japan. (English and
579 Japanese)
580 van Gelder HA, Poorter L, Sterck FJ (2006) Wood mechanics, allometry, and life-
581 history variation in a tropical rain forest tree community. New Phytol 171:367–
582 378. doi: 10.1111/j.1469-8137.2006.01757.x.
583 Gibert A, Gray EF, Westoby M, et al (2016) On the link between functional traits and
584 growth rate: meta-analysis shows effects change with plant size, as predicted. J
585 Ecol 104:1488–1503. doi: 10.1111/1365-2745.12594
586 Givnish TJ (1988) Adaptation to sun and shade: a whole-plant perspective. Australian
587 Journal of Plant Physiology 15:63–92. doi: 10.1071/PP9880063
588 Grime JP, Thompson K, Hunt R, et al (1997) Integrated screening validates primary

589 axes of specialisation in plants. Oikos 79:259–281. doi: 10.2307/3546011
590 Hacke UG, Spicer R, Schreiber SG, Plavcová L (2017) An ecophysiological and
591 developmental perspective on variation in vessel diameter. Plant, Cell &
592 Environment 40: 831-845. doi: 10.1111/pce.12777
593 Hietz P, Rosner S, Hietz-Seifert U, Wright SJ (2017) Wood traits related to size and life
594 history of trees in a Panamanian rainforest. New Phytologist 213:170–180. doi:
595 10.1111/nph.14123
596 Hinckley TM, Duhme F, Hinckley AR, Richter H (1980) Water relations of drought
597 hardy shrubs: osmotic potential and stomatal reactivity. Plant, Cell & Environment
598 3:131–140. doi: 10.1111/1365-3040.ep11580919
599 Hiura T, Yoshioka H, Matsunaga SN, Saito T, Kohyama TI, Kusumoto N, Uchiyama K,
600 Suyama Y, Tsumura Y (2021) Diversification of terpenoid emissions proposes a
601 geographic structure based on climate and pathogen composition in Japanese cedar.
602 Scientific Reports 11:8307. doi: 10.1038/s41598-021-87810-x
603 Hunt R (1978) Plant growth analysis. Studies in biology no. 96. E Arnold.
604 Hunt R (1982) Plant growth curves. Edward Arnold, London.
605 Iida Y, Kohyama TS, Swenson NG, et al (2014) Linking functional traits and
606 demographic rates in a subtropical tree community: The importance of size

607 dependency. Journal of Ecology 102:641–650. doi: 10.1111/1365-2745.12221
608 Inoue Y., Kitaoka, K., Araki, M., Kenzo, T., Saito S. (2018) Seasonal changes in leaf
609 water potential, photosynthetic and transpiration rates in upper canopy needles in
610 *Cryptomeria japonica*. Kanto Japanese Forest Research 69: 19–22. (In Japanese
611 with English summary).
612 Ishii H, Asano S (2010) The role of crown architecture, leaf phenology and
613 photosynthetic activity in promoting complementary use of light among coexisting
614 species in temperate forests. Ecological Research 25:715–722. doi:
615 10.1007/s11284-009-0668-4
616 Ishii H, Takashima A, Makita N, Yoshida S (2010) Vertical stratification and effects of
617 crown damage on maximum tree height in mixed conifer-broadleaf forests of
618 Yakushima Island, southern Japan. Plant Ecology 211:27–36. doi: 10.1007/s11258-
619 010-9768-z
620 Ishii HR, Horikawa Shin-ichiro, Noguchi Y, Azuma W (2018) Variation of intra-crown
621 leaf plasticity of *Fagus crenata* across its geographical range in Japan. Forest
622 Ecology and Management 429:437–448. doi: 10.1016/j.foreco.2018.07.016
623 Itaka S, Yoshida S, Mizoue N, Ota T, Takashima A, Kajisa T, Yasue K (2013) Estimation
624 of growth rates based on tree-ring analysis of *Cryptomeria japonica* on Yakushima

625 Island, Japan. Journal of Forest Planning 19:1–7. doi: 10.20659/jfp.19.1_1
626 Kanda T, Takata Y, Kohyama K, Ohkura T, Maejima Y, Wakabayashi S, Obara H (2018)
627 New soil maps of Japan based on the comprehensive soil classification system of
628 Japan – first approximation and its application to the world Reference Base for soil
629 resources 2006. Japan Agricultural Research Quarterly 49:217–226. doi:
630 10.6090/jarq.52.285
631 King DA, Davies SJ, Tan S, Noor NSM (2006) The role of wood density and stem
632 support costs in the growth and mortality of tropical trees. Journal of Ecology
633 94:670–680. doi: 10.1111/j.1365-2745.2006.01112.x
634 Kitajima K (1994) Relative importance of photosynthetic traits and allocation patterns
635 as correlates of seedling shade tolerance of 13 tropical trees. Oecologia 98:419–
636 428. doi: 10.1007/BF00324232
637 Kobayashi, H., Inoue, S. & Gyokusen, K. (2010) Spatial and temporal variations in the
638 photosynthesis-nitrogen relationship in a Japanese cedar (*Cryptomeria japonica* D.
639 Don) canopy. Photosynthetica, 48, (2), 249−256. doi: 10.1007/s11099-010-0031-6
640 Liu, H., Gleason, S. M., Hao, G., Hua, L., He, P., Goldstein, G. & Ye, Qing. (2019)
641 Hydraulic traits are coordinated with maximum plant height at the global scale.
642 Science Advances, 5, eaav1332. doi: 10.1126/sciadv.aav1332

643 Martínez-Vilalta J, Mencuccini M, Vayreda J, Retana J (2010) Interspecific variation in
644 functional traits, not climatic differences among species ranges, determines
645 demographic rates across 44 temperate and Mediterranean tree species. Journal of
646 Ecology 98:1462–1475. doi: 10.1111/j.1365-2745.2010.01718.x
647 Medeiros CD, Scoffoni C, John GP, et al (2019) An extensive suite of functional traits
648 distinguishes Hawaiian wet and dry forests and enables prediction of species vital
649 rates. Functional Ecology 33:712–734. doi: 10.1111/1365-2435.13229
650 Messier J, McGill BJ, Lechowicz MJ (2010) How do traits vary across ecological
651 scales? A case for trait-based ecology. Ecological Letter 13:838–848. doi:
652 10.1111/j.1461-0248.2010.01476.x
653 Montgomery RA, Chazdon RL (2002) Light gradient partitioning by tropical tree
654 seedlings in the absence of canopy gaps. Oecologia 131:165–174. doi:
655 10.1007/s00442-002-0872-1
656 Moreira X, Mooney KA, Rasmann S, et al (2014) Trade-offs between constitutive and
657 induced defences drive geographical and climatic clines in pine chemical defences.
658 Ecological Letter 17:537–546. doi: 10.1111/ele.12253
659 Nabeshima E, Kubo T, Hiura T (2010) Variation in tree diameter growth in response to
660 the weather conditions and tree size in deciduous broad-leaved trees. Forest and

661 Ecological Management 259:1055–1066. doi: 10.1016/j.foreco.2009.12.012
662 Nakagawa S, Schielzeth H (2013) A general and simple method for obtaining R^2 from
663 generalized linear mixed-effects models. Methods Ecology and Evolution 4:133–
664 142. doi: 10.1111/j.2041-210x.2012.00261.x
665 Niinemets Ü (2010) A review of light interception in plant stands from leaf to canopy in
666 different plant functional types and in species with varying shade tolerance.
667 Ecological Research 25:693–714. doi: 10.1007/s11284-010-0712-4
668 Nishizono T, Kitahara F, Iehara T, Mitsuda Y (2014) Geographical variation in age-
669 height relationships for dominant trees in Japanese cedar (*Cryptomeria japonica* D.
670 Don) forests in Japan. Journal of Forest Research 19:305–316. doi:
671 10.1007/s10310-013-0416-z
672 Norman J, Welles J, McDermitt D (1992) Estimating canopy light-use and transpiration
673 efficiencies from leaf measurements. In: Inc. L-C (ed) Li-Cor Application Note
674 #105. Lincoln, NE
675 Obeso JR (2002) The costs of reproduction in plants. New Phytologist 155:321–348.
676 doi: 10.1046/j.1469-8137.2002.00477.x
677 Ohta T, Niwa S, Hiura T (2019) Geographical variation in Japanese cedar shapes soil
678 nutrient dynamics and invertebrate community. Plant and Soil 437:355–373. doi:

679 10.1007/s11104-019-03983-5
680 Olson ME, Anfodillo T, Gleason SM, McCulloh KA (2021) Tip-to-base xylem conduit
681 widening as an adaptation: causes, consequences, and empirical priorities. New
682 Phytologist 229: 1877-1893. doi: 10.1111/nph.16961
683 Olson ME, Anfodillo T, Rosell JA, et al (2014) Universal hydraulics of the flowering
684 plants: Vessel diameter scales with stem length across angiosperm lineages, habits
685 and climates. Ecological Letter 17:988–997. doi: 10.1111/ele.12302
686 Olson ME, Soriano D, Rosell JA, et al (2018) Plant height and hydraulic vulnerability to
687 drought and cold. Proceedings of the National Academy of Sciences of the United
688 States of America 115:7551–7556. doi: 10.1073/pnas.1721728115
689 Onoda Y, Saluñga JB, Akutsu K, et al (2014) Trade-off between light interception
690 efficiency and light use efficiency: Implications for species coexistence in one-
691 sided light competition. Journal of Ecology 102:167–175. doi: 10.1111/1365-
692 2745.12184
693 Osada N, Nabeshima E, Hiura T (2015) Geographic variation in shoot traits and
694 branching intensity in relation to leaf size in Fagus crenata: a common garden
695 experiment. American Journal of Botany 102:878–887. doi: 10.3732/ajb.1400559
696 Osone Y, Hashimoto S, Kenzo T (2021) Verification of our empirical understanding of

697 the physiology and ecology of two contrasting plantation species using a trait
698 database. PLoS One 16:274–275. doi: 10.1371/journal.pone.0254599
699 Parker WC, Colombo SJ (1995) A critical re-examination of pressure-volume analysis
700 of conifer shoots: comparison of three procedures for generating PV curves on
701 shoots of *Pinus resinosa* Ait. seedlings. Journal of Experimental Botany 46:1701–
702 1709.
703 Petit G, Anfodillo T, Mencuccini M (2008) Tapering of xylem conduits and hydraulic
704 limitations in sycamore (*Acer pseudoplatanus*) trees. New Phytologist 177:653–
705 664. doi: 10.1111/j.1469-8137.2007.02291.x
706 Poorter H, Jagodzinski AM, Ruiz-Peinado R, et al (2015) How does biomass
707 distribution change with size and differ among species? An analysis for 1200 plant
708 species from five continents. New Phytologist 208:736–749. doi:
709 10.1111/nph.13571
710 Poorter H, Remkes C (1990) Leaf area ratio and net assimilation rate of 24 wild species
711 differing in relative growth rate. Oecologia 83:553–559.
712 Poorter L, Bongers F, Sterck FJ, Wöll H (2003) Architecture of 53 rain forest tree
713 species differing in adult stature and shade tolerance. Ecology 84:602–608.
714 Poorter L, Bongers L, Bongers F (2006) Architecture of 54 moist forest tree species:

715 traits, trade-offs, and functional groups. Ecology 87:1289–1301. doi: 10.1890/07-
716 0207.1
717 Poorter L, McDonald I, Alarcón A, et al (2010) The importance of wood traits and
718 hydraulic conductance for the performance and life history strategies of 42
719 rainforest tree species. New Phytologist 185:481–492.
720 R core Team (2019) R: A language and environment for statistical computing. R
721 Foundation for Statistical Computing.
722 Reich PB (2014) The world-wide 'fast-slow' plant economics spectrum: a traits
723 manifesto. Journal of Ecology 102:275–301. doi: 10.1111/1365-2745.12211
724 Rosell JA, Olson ME, Anfodillo T (2017) Scaling of xylem vessel diameter with plant
725 size: causes, predictions, and outstanding questions. Current Forestry Reports
726 3:46–59. doi: 10.1007/s40725-017-0049-0
727 Ryan MG, Yoder BJ (1997) Hydraulic limits to tree height and tree growth: What keeps
728 trees from growing beyond a certain height? Bioscience 47:235–242. doi:
729 10.2307/1313077
730 Santiago LS, Goldstein G, Meinzer FC, et al (2004) Leaf photosynthetic traits scale
731 with hydraulic conductivity and wood density in Panamanian forest canopy trees.
732 Oecologia 140:543–550. doi: 10.1007/s00442-004-1624-1

733 Schindelin J, Arganda-Carreras I, Frise E, et al (2012) Fiji: an open-source platform for
734 biological-image analysis. Nature Methods 9:676–82. doi: 10.1038/nmeth.2019
735 Schneider CA, Rasband WS, Eliceiri KW (2012) NIH Image to ImageJ: 25 years of
736 image analysis. Nature Methods 9:671–675. doi: 10.1038/nmeth.2089
737 Shinozaki K, Yoda K, Hozumi K, Kira T (1964) A quantitative analysis of plant form-
738 the pipe model theory I. Basic analyses. Japanese Journal of Ecology 14:97–105.
739 doi: 10.1086/368398
740 Sperry JS (2003) Evolution of water transport and xylem structure. International Journal
741 of Plant Science 164:115–S127. doi: 10.1086/368398
742 Sperry JS, Adler FR, Campbell GS, Comstock JP (1998) Limitation of plant water use
743 by rhizosphere and xylem conductance: Results from a model. Plant, Cell and
744 Environment 21:347–359. doi: 10.1046/j.1365-3040.1998.00287.x
745 Spicer R, Gartner BL (2001) The effects of cambial age and position within the stem on
746 specific conductivity in Douglas-fir (*Pseudotsuga menziesii*) sapwood. Trees –
747 Structure and Function 15:222–229. doi: 10.1007/s004680100093
748 Stenberg P (1996) Simulations of the effects of shoot structure and orientation on
749 vertical gradients in intercepted light by conifer canopies. Tree Physiology 16:99–
750 108. doi: 10.1093/treephys/16.1-2.99

751 Takashima A, Kume A, Yoshida S, et al (2009) Discontinuous DBH-height relationship
752 of *Cryptomeria japonica* on Yakushima Island: Effect of frequent typhoons on the
753 maximum height. Ecological Research 24:1003–1011. doi: 10.1007/s11284-008-
754 0574-1
755 Tateishi M, Kumagai T, Suyama Y, Hiura T (2008) Differences in transpiration
756 characteristics of Japanese beech trees, *Fagus crenata*, in Japan. Tree Physiology
757 30: 748-760. doi: 10.1093/treephys/tpq023
758 Tobita H, Kitao M, Saito T, Kabeya D, Kawasaki T, Yazaki K, Komatsu M and
759 Kajimoto T. (2014) Seasonal variation of photosynthetic parameters within a
760 *Crypyomeria japonica* crown. Kanto Japanese Forest Research 65: 103–106. (In
761 Japanese with English summary).
762 Tsumura Y, Uchiyama K, Moriguchi Y, et al (2012) Genome scanning for detecting
763 adaptive genes along environmental gradients in the Japanese conifer, *Cryptomeria*
764 *japonica*. Heredity (Edinb) 109:349–360. doi: 10.1038/hdy.2012.50
765 Tsumura Y, Uchiyama K, Moriguchi Y, et al (2014) Genetic differentiation and
766 evolutionary adaptation in *Cryptomeria japonica*. G3 Genes|Genomes|Genetics
767 4:2389–2402. doi: 10.1534/g3.114.013896
768 Tyree MT, Hammel HT (1972) The measurement of the turgor pressure and the water

769 relations of plants by the pressure-bomb technique. Journal of Experimental
770 Botany 23:267–282.
771 Tyree MT, Zimmermann MH (2002) Xylem structure and the ascent of sap, Ed. 2.
772 Springer-Verlag, Berlin.
773 West GB, Brown JH, Enquist BJ (1999) A general model for the structure and allometry
774 of plant vascular systems. Nature 400:664–667. doi: 10.1038/23251
775 Williams CB, Anfodillo T, Crivellaro A, et al (2019) Axial variation of xylem conduits
776 in the Earth's tallest trees. Trees – Structure and Function 33:1299–1311. doi:
777 10.1007/s00468-019-01859-w
778 Wright SJ, Kitajima K, Kraft NJB, et al (2010) Functional traits and the growth–
779 mortality trade-off in tropical trees. Ecology 91:3664–3674. doi: 10.1890/09-
780 2335.1
781 Wu QS, Xia RX (2006) Arbuscular mycorrhizal fungi influence growth, osmotic
782 adjustment and photosynthesis of citrus under well-watered and water stress
783 conditions. Journal of Plant Physiology 163:417–425. doi:
784 10.1016/j.jplph.2005.04.024.
785 Zheng, J., Li, Y., Morris, H., Vandelook, F. & Jansen, S. (2022) Variation in t racheid
786 dimensions of conifer xylem reveals evidence of adaptation to environmental

787 conditions. Fronters in Plant Science, 13, 774241. doi: 10.3389/fpls.2022.774241

Table 1. Comparisons of growth and relative growth rate (RGR) for height and diameter at breast heigh (DBH) in trees from 2013 to 2016, including mean values, standard errors, and the results of linear mixed model analysis for three provenances (Yaku, Yanase, and Yoshino) of *Cryptomeria japonica*. G_h: growth rate for height, Gr: growth rate for DBH, RGR_h: relative growth rate for height, RGR_r: relative growth rate for DBH.

	G_h	G_r	RGR_h	RGR_r
Unit	cm yr^{-1}	mm yr^{-1}	10^{-3} yr^{-1}	10^{-3} yr^{-1}
Yaku	5.6 (1.6) b	0.36 (0.11) b	6.08 (1.76) b	2.70 (0.80) c
Yanase	20.5 (6.1) a	1.00 (0.29) a	10.72 (3.16) a	5.60 (1.62) a
Yoshino	15.1 (4.5) a	0.95 (0.28) a	9.12 (2.72) ab	3.92 (1.14) b

Different letters indicate significant differences between parameters among provenances ($p < 0.05$).

Table 2. Comparisons of leaf, stem, and whole-tree traits among three provenances of *Cryptomeria. japonica*, including mean values, standard errors, and results of one-way ANOVA or Kruskal–Wallis test.

Trait	Symbol	Unit	Cultivars of *C. japonica*			*p* value
			Yaku	Yanase	Yoshino	
Tree structures						
Crown depth	CD	m	3.18 (0.89) b	10.89 (1.23) a	7.53 (0.80) ab	0.012
Ratio of crown depth to tree height	RCD	$m\ m^{-1}$	0.27 (0.09)	0.52 (0.08)	0.36 (0.05)	0.142
Total branch cross-sectional area per stem volume	TBA	$cm^2\ m^{-3}$	929 (170) a	594 (36) ab	439 (46) b	0.021
Sapwood density	WD	$g\ cm^{-3}$	0.39 (0.01) a	0.34 (0.01) b	0.33 (0.01) b	< 0.001
Whole-tree hydraulic architecture						
Daytime water potential of treetop leaves	Ψ_{TL}	MPa	–1.14 (0.09)	–1.33 (0.06)	–1.31 (0.06)	0.182

Daytime water potential of lowest-crown leaves	Ψ_{LL}	MPa	–1.05 (0.10)	–1.20 (0.10)	–1.24 (0.04)	0.322
Daytime water potential of fine-roots [1]	Ψ_{R}	MPa	–0.34 (0.08)	–0.20 (0.06)	–0.19 (0.01)	0.146
Water potential difference between root and treetop	$\Psi_{R} - \Psi_{TL}$	MPa	0.80 (0.13)	1.13 (0.12)	1.12 (0.05)	0.113
Axial variation-weighted potential specific xylem conductance	K_{ap}	kg m^{-2} s^{-1} MPa^{-1}	1.19 (0.06) a	0.68 (0.02) b	0.63 (0.04) b	< 0.001
Potential transpiration rate per unit sapwood area	E_p	kg m^{-2} s^{-1}	0.93 (0.13)	0.77 (0.05)	0.71 (0.06)	0.278
Leaf water relations						
Osmotic potential at turgor loss [1]	Ψ_{tlp}	MPa	–2.08 (0.20)	–1.64 (0.17)	–2.06 (0.13)	0.430
Osmotic potential at saturation [1]	Ψ_{sat}	MPa	–1.43 (0.08)	–1.09 (0.26)	–1.45 (0.02)	0.731
Relative water content at turgor loss	RWC_{tlp}	gH_2O gH_2O^{-1}	0.76 (0.03)	0.76 (0.01)	0.69 (0.02)	0.068

Leaf hydraulic capacitance	C_L	mol m^{-2} MPa^{-1}	1.52 (0.22)	1.85 (0.30)	1.94 (0.24)	0.524
Leaf succulence	S_L	gH_2O m^{-2}	204 (38)	228 (23)	241 (25)	0.687
Leaf morphology						
Leaf dry mass per area ratio [1]	LMA	g m^{-2}	411 (36)	321 (1)	385 (40)	0.061
Shoot silhouette area to projected leaf area ratio [1]	SPAR	m^2 m^{-2}	0.64 (0.01)	0.68 (0.03)	0.74 (0.05)	0.113
Leaf photosynthesis						
Maximum net photosynthetic rate	P_{max}	µmol CO_2 m^{-2} s^{-1}	3.56 (0.26)	3.17 (0.28)	4.05 (0.14)	0.095
Maximum net photosynthetic rate per leaf dry mass	P_{max_mass}	nmol CO_2 g^{-1} s^{-1}	8.69 (0.14)	9.87 (0.84)	10.76 (1.28)	0.319
Dark respiration rate [1]	R	µmol CO_2 m^{-2} s^{-1}	0.62 (0.02)	0.48 (0.09)	0.80 (0.09)	0.042
Light compensation point [1]	L_C	µmol PPFD m^{-2} s^{-1}	21.5 (1.1)	12.5 (4.9)	46.7 (12.9)	0.053
Stable carbon isotope ratio	$\delta^{13}C$	‰	–28.8 (0.27)	–29.7 (0.21)	–29.5 (0.33)	0.054

Dry-mass based carbon concentration [1]	C_{mass}	%	54.0 (0.24)	53.3 (0.35)	53.2 (0.47)	0.200
Dry-mass based nitrogen concentration	N_{mass}	%	1.10 (0.04)	1.28 (0.06)	1.21 (0.07)	0.111

Significant differences between provenances are denoted by different letters (Tukey's HSD or Steel–Dwass test, $p < 0.05$)

[1] Differences in means among provenances were examined by Kruskal–Wallis test.

Table 3. Estimation of slopes (β) and intercepts (α) for the relationships between $\log_{10}$-transformed distance from tree apex (L) and hydraulically-weighted tracheid diameter (D_h) based on the linear mixed models for three provenances (Yaku, Yanase, and Yoshino) of *Cryptomeria japonica*.

	Slope (β)	Intercept (α)
Yaku	0.070 (0.016) b	1.354 (0.012) a
Yanase	0.171 (0.023) a	1.272 (0.021) b
Yoshino	0.130 (0.022) a	1.292 (0.019) b

Values in parentheses represent standard errors.

Different letters indicate significant differences in parameters among provenances ($p < 0.05$).

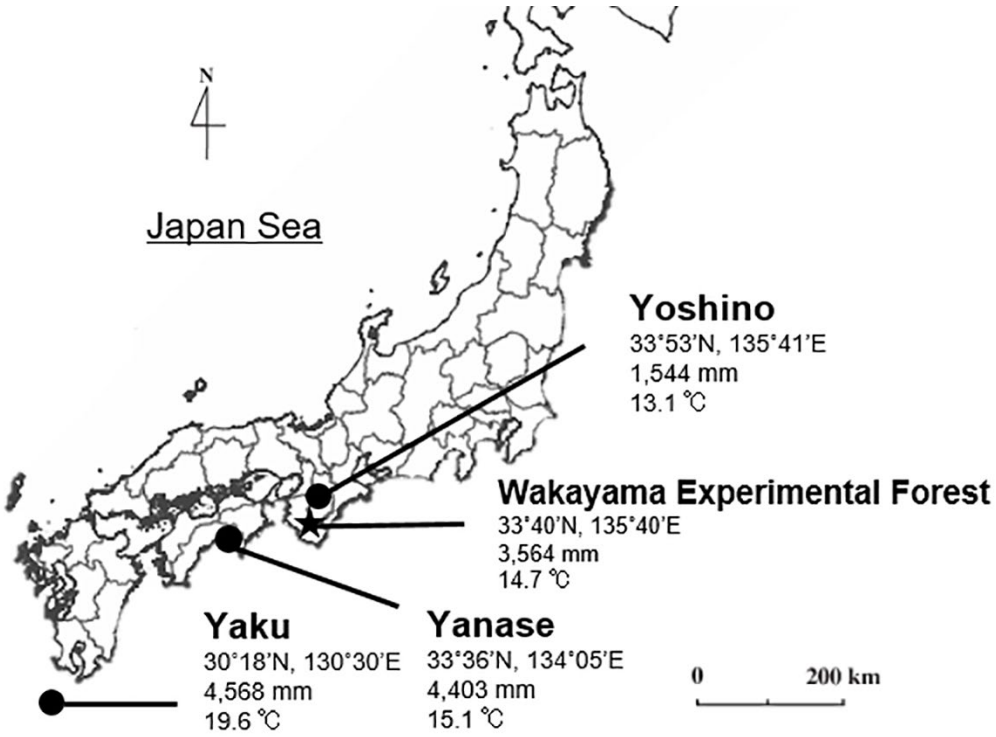

Figure 1. Location (latitude and longitude), mean annual temperature, and mean annual precipitation of the common garden of the present study (Wakayama Experimental Forest) and the native habitats of three provenances (Yoshino, Yanase, and Yaku). The location of the native habitats of three provenances shows the source location of each sapling planted in the common garden. The mean annual temperature and precipitation were calculated from observations from 1985 to 2019 at the nearest Japan Meteorological Agency weather station to that location.

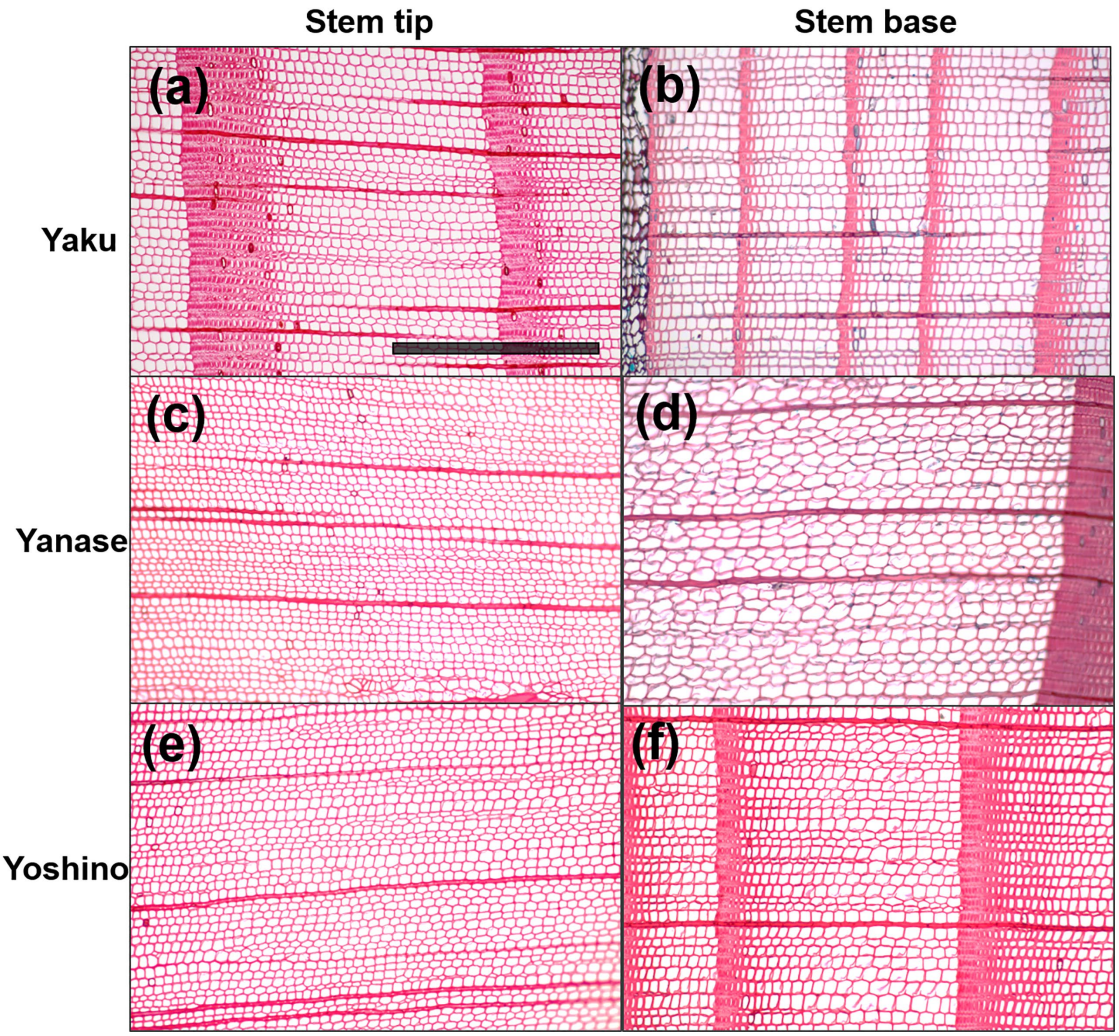

Figure 2. Optical microscopic images of stained transverse sections of the xylem at the stem tips (a, c, e) and bases (b, d, f) of three provenances of *Cryptomeria japonica*: Yaku (a, b), Yanase (c, d), and Yoshino (e, f). All images are at the same magnification (bar = 500 μm). The pith is on the right side in each image.

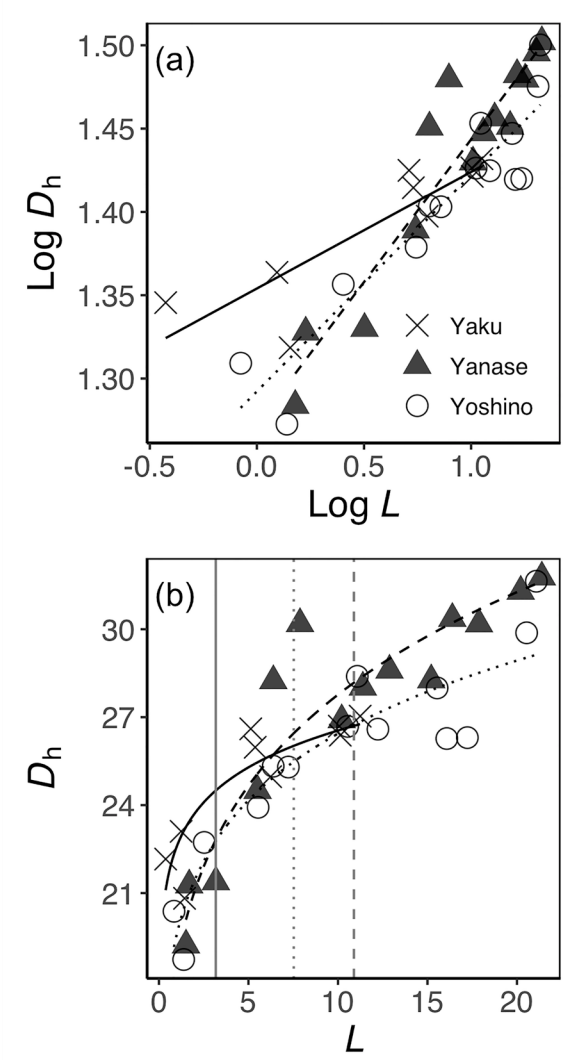

Figure 3. (a) Scaling relationships between $\log_{10}$-transformed hydraulically-weighted tracheid diameter (D_h) and distance from tree apex (L) for three provenances (Yaku, Yanase, and Yoshino) of *Cryptomeria japonica*. Solid, dashed, and dotted lines indicate the trends for Yaku, Yanase, and Yoshino, respectively. On average, the provenance with a steeper slope (β) had a longer crown depth (CD) (R^2 = 0.999, p = 0.021, n = 3). (b) The same data in non-transfomed axes. The vertical solid, dashed, and dotted lines indicate the aveage CD (see also Table 1) for Yaku, Yanase, and Yoshino, respectively. Each symbol is a composite of multiple individuals (n = 3 for each provenance).